Macromolecules

ARTICLE

pubs.acs.org/Macromolecules

# Supramolecular Hybrid Hydrogels from Noncovalently Functionalized Graphene with Block Copolymers

Jianghua Liu, Guosong Chen,* and Ming Jiang*

The Key Laboratory of Molecular Engineering of Polymers, Ministry of Education and Department of Macromolecular Science, Fudan University, 220 Handan Road, Shanghai 200433, China

Supporting Information

**ABSTRACT:** In recent years, graphene has become a prevailing topic in the materials community. Numerous applications of graphene have been generated, including gas sensors, photovoltaics, field-effect transistors, *etc.* In this paper, we demonstrate that graphene sheets could serve as a desirable inorganic constituent in constructing hybrid polymeric hydrogels via supramolecular routes, which currently is not so popular as the other applications. In this paper, graphene oxide (GO) nanosheets were modified by grafting $\beta$-cyclodextrins first, leading to chemical converted graphene (CCG), and then noncovalently functionalized by block copolymers AZO-PDMA-*b*-PNIPAM via inclusion complexation. The resulted hybrid graphene inclusion complex (HGIC) was fully characterized by a combination of techniques including UV−vis spectroscopy, thermogravimetric analysis (TGA), X-ray photoelectron spectroscopy (XPS), Raman spectroscopy, atomic force microscopy (AFM), and transmission electron microscopy (TEM). Then, due to the thermo sensitivity of the PNIPAM block, HGIC solutions exhibited sol−gel transition at elevated temperature. Rheology studies revealed that the gelation of the HGIC suprastructure took place much faster at a temperature close to but lower than the LCST of PNIPAM. It was also found that the gelation temperature increased with the ratio of degree of polymerization of PDMA block to PNIPAM block of HGIC suprastructures. On the basis of the results, a new possible gelation mechanism was proposed. The flexible and ultrathin 2D planar structure of graphene sheets exhibited unprecedented advantage in constructing the 3D network structure of the hydrogels, showing rapid sol−gel transition at elevated temperature.

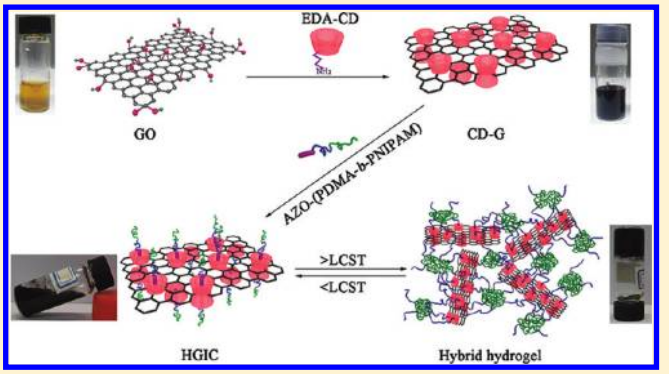


## INTRODUCTION

Recently, an extension of the concept of "organic/inorganic nanocomposites" to the field of polymeric hydrogels has made great successes. The obtained novel soft materials are very promising because of the significant improvement of their properties compared to their organic and inorganic precursors.[1] For example, introducing clay nanoplatelets into the synthetic polymeric network remarkably improved the mechanical properties of the resultant hybrid hydrogels.[1a] And incorporating surface-functionalized inorganic nanoparticles was found effective in promoting the hydrogel formation of pseudopolyrotaxane and improving the strength.[2]

Currently, as the youngest and probably the most attractive inorganic nanomaterial, graphene leads to an explosion of scientific creativity and productivity, due to its single-atom thickness, flexible two-dimensional (2D) structure and exceptional physical and chemical properties.[3] The great success of employing graphene inspires us to try to incorporate it into polymeric hydrogels. Although there are quite a few reports using graphene oxide (GO), the well-known chemical precursor of graphene to make "organic/inorganic nanocomposite" hydrogels,[4] as far as we know, using graphene, or chemical converted graphene (CCG), as the inorganic nanocomponent to make hybrid polymeric hydrogels is limited.[5,6] Graphene was introduced to the hydrogel of pseudopolyrotaxane between cyclodextrin and pluronic polymer, resulting in a hybrid hydrogel with thermo responsiveness but decreased viscosity and strength compared to the native one.[6]

More and more investigators have employed exfoliation and reduction of GO for large-scale production of graphene, especially for the preparation of polymer composites.[7] GO is a layered material produced by the oxidation of graphite. It is heavily oxygenated, bearing hydroxyl, carboxyl, and epoxide groups on its basal planes,[8,9] which enable GO to be further functionalized through covalent or noncovalent approaches. A number of methods have been reported for generating polymers directly from graphene sheets using GO as precursor.[10]

A systematic research about polymeric hydrogels incorporating various supramolecular factors has been performed in our group. For example, we utilized the well-known host−guest pairs

**Received:** July 14, 2011
**Revised:** August 13, 2011
**Published:** September 14, 2011

Scheme 1. Synthetic Route of CD-G and the Corresponding Photos of Aqueous Solutions of GO and CD-G

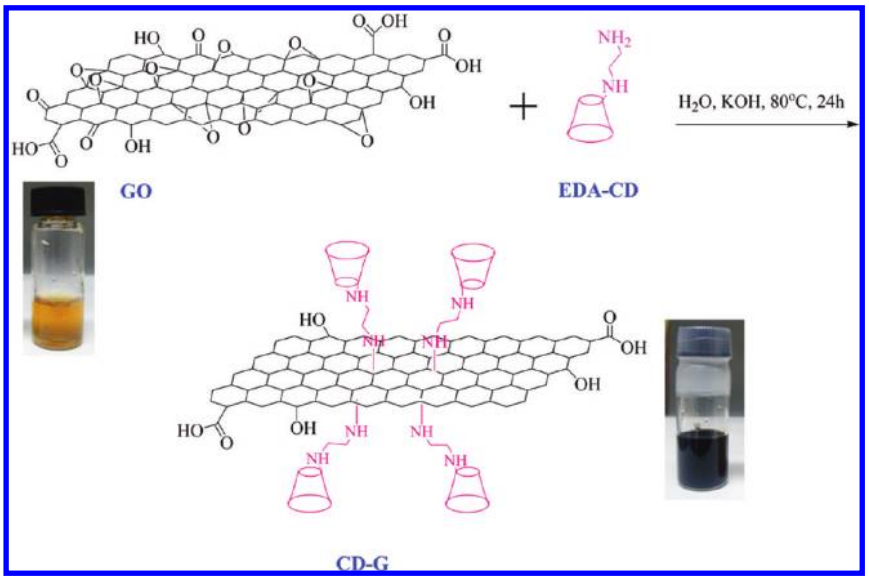


based on cyclodextrins (CDs), as the linkage between the CD-modified inorganic components and polymer chains.[2,11,12] Thus, the CD-coated nanoparticles led the guest-functionalized polymer chains into hydrogels. In this paper, we designed and synthesized CD-modified graphene via amine-epoxy reaction of GO. Using azobenzene end modified block copolymer poly(*N*,*N*-dimethylacrylamide)-*b*-poly(*N*-isopropylacrylamide) (AZO-PDMA-*b*-PNIPAM), we successfully prepared block copolymer grafted graphene sheets via inclusion complexation for the first time. The resultant hybrid graphene inclusion complex (HGIC) turned into supramolecular polymeric hydrogels upon heating. The gelation behavior depended on the structure of the block copolymers. Therefore, graphene was proved to be a promising and unique inorganic nanocomponent for fabricating hybrid polymeric hydrogels, due to its large and flexible 2D structure.

## RESULTS AND DISCUSSION

**Preparation of CD Attached Graphene (CD-G) and the Subsequent Noncovalent Modification with Block Copolymers.** GO has been prepared by modified Hummers' oxidation method[13] of graphite. Several different chemical strategies have been reported to open the epoxide ring on GO and restore the $sp^2$ planar surface with new functionalities.[9] In this work, ethylenediamino-$\beta$-cyclodextrin (EDA-CD) as a nucleophile has been covalently attached to graphene surface via amine-epoxy reaction (Scheme 1). As far as we know, demonstration of CD functionalized graphene is very limited,[14] where native CDs were employed to react with GO. Because of the stronger nucleophilicity of amines in EDA-CDs than hydroxyl groups of native $\beta$-CD, the amine-epoxy reaction was expected to be more effective to introduce CDs than that of using native CDs. Although two synthetic steps are required to prepare EDA-CD, they are well-setup procedures and our results below demonstrate the efficiency of this amine-epoxy reaction. CD-G is prepared by mixing GO and EDA-CD in the solution of KOH at 80 °C for 24 h.[15] As shown in Scheme 1, the obtained CD-G solution is dark and homogeneous showing well dispersion of the graphene sheets. After extra EDA-CD and ions were removed by dialysis, the CD-G solid product was obtained through centrifugation or lyophilization from water, which was long-term stable and homogeneously dispersed in water without any precipitation after ultrasonic treatment. The concentration of CD-G can even reach 20 mg/mL. It is worth to mention that, although dispersion of CD-G in neutral water shows satisfactory stability, water at pH 8−9 (adjusted by NaOH) is the optimized medium, since the hydroxide anion can break the inter- or intramolecular hydrogen bonds of CDs and increase their water solubility.

In our previous reports, $\beta$-CDs were successfully used to functionalize the surface of silica nanoparticles[2] and quantum dots.[11] Then, homopolymers or block copolymers with guest species at one of their ends were attached onto the particle surface via inclusion complexation. The obtained suprastructure with the inorganic particle as its core and copolymers as its shell was named a hybrid inclusion complex (HIC).[11] In this paper, an extension from the nanoparticle-based HIC to hybrid graphene inclusion complex (HGIC) was successfully performed. A series of AZO-(PDMA-*b*-PNIPAM) copolymers with different polymerization degrees (DP) of the blocks via RAFT polymerization were prepared (synthetic route in Figure S1, Supporting Information). The polymerization was initiated from an AZO functionalized chain transfer agent (CTA), where AZO served a guest moiety to $\beta$-CD. In early literature,[16] the binding constant between $\beta$-CD and water-soluble AZO derivative was measured to be 2000 $M^{-1}$. Hydrophilic PDMA chain and thermo sensitive PNIPAM chain were installed subsequently. The obtained copolymers with narrow molecular weight distribution were characterized by GPC and $^1$H NMR, as shown in our previous report[11a] and Figures S2 and S3 (Supporting Information) in this paper. When CD-G and the copolymer were mixed in water (molar ratio of CD vs AZO 1:1, pH 8−9), the attachment of copolymer to graphene surface took place and HGIC suprastructure formed because of the inclusion complexation between CD and AZO. HGIC can easily be purified from CD-G via low speed centrifugation, since the weight of the nanosheets increased abruptly due to the copolymer attachment.

**Characterization and Structure Analysis of GO, CD-G, and HGIC.** In this section, the characterization data of GO, CD-G, and

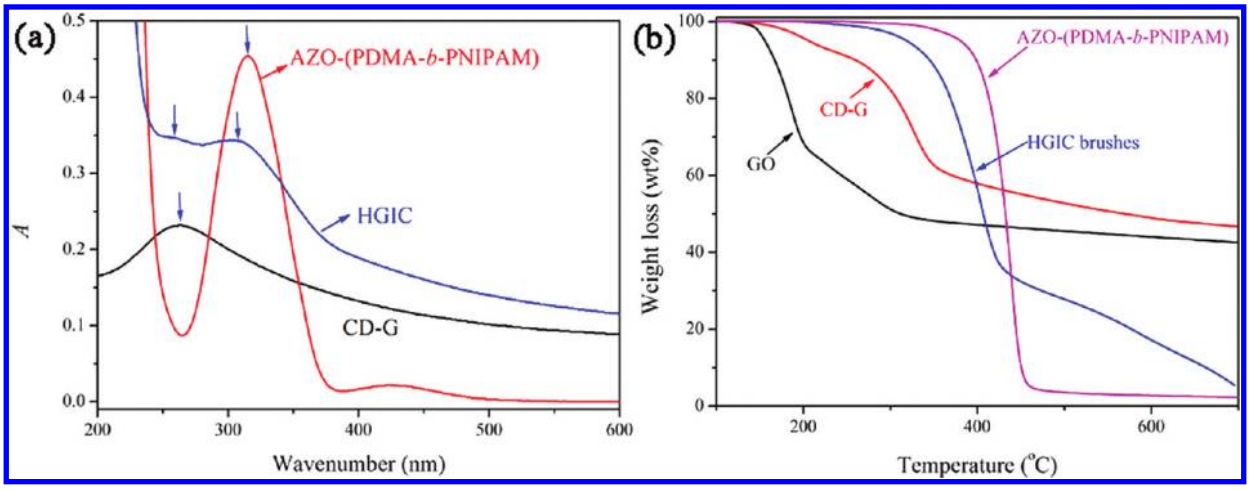


**Figure 1.** (a) UV/vis absorption spectra of CD-G, HGIC, and AZO-(PDMA-*b*-PNIPAM) block copolymer **P3** and (b) TGA curves of GO, CD-G, HGIC, and copolymer **P3**. TGA was measured at the heating rate of 20 °C/min under nitrogen.

HGIC from UV−vis spectra, TGA, Raman spectra, XPS, AFM, and TEM are discussed. The HGIC samples have been made from seven block copolymers. In this part, copolymer AZO-($PDMA_{104}$-*b*-$PNIPAM_{138}$) (**P3**) is taken as an example to demonstrate the HGIC structure. HGIC samples have been carefully centrifuged and washed in order to remove the free copolymers for further characterization. Figure 1a shows the UV−vis spectra of CD-G, copolymer **P3** and HGIC. CD-G has an absorption peak at 263 nm with hyperchromicity over the entire scan range.[17] The copolymer has characteristic absorption peaks at 315 and 420 nm, which can be attributed to the characteristic intense $\pi-\pi^*$ transition and weak $n-\pi^*$ transition of AZO group, respectively.[18] In the UV−vis spectrum of HGIC, the characteristic absorption peaks inherited from CD-G and AZO are slightly weakened and blue-shifted, *i.e.*, the absorption peak from CD-G moves from 263 to 255 nm ($\Delta\lambda$ = 8 nm), while that from AZO units shifts from 315 to 303 nm ($\Delta\lambda$ = 12 nm). This result clearly proves the inclusion complexation between $\beta$-CDs on CD-G and AZO moieties of copolymers.

Another evidence of inclusion complexation came from TGA. First of all, the successful covalent functionalization of GO with EDA-CD was verified. As shown in Figure 1b, GO was thermally unstable and more than 30% of its weight loss took place even below 200 °C, which was assigned to the decomposition of the labile oxygen-containing functional groups.[19] However, CD-G, of which the labile groups had been removed via covalent attachment of GO with EDA-CD, showed weight loss only less than 10% below 250 °C. Then a major weight loss of 35% in the range from 250 to 450 °C followed, as a result of decomposition of CDs on the graphene sheet. Similar decomposition temperature of EDA-CD itself (Figure S4, Supporting Information) confirmed this assignment. Finally there was a very slow weight-loss process of CD-G, from 450 to 700 °C, which was due to the partial decomposition of graphene sheet itself. Generally, CD-G showed an obvious better thermo-stability than GO, which could be attributed to the removal of the easily decomposable oxygen-containing residuals by amine-epoxy reaction. It is worth to mention that, the weight loss attributed to CDs here is larger than that of the native CD-modified graphene previously reported.[14] This result clearly proves the high efficiency of amine moiety of EDA-CD to react with epoxide on GO in our experiment.

Furthermore, as shown in Figure 1b, the TGA data of HGIC gives some information about the suprastructure based on inclusion complexation. There are two major mass losses of HGIC. The first is about 69% from 300 to 420 °C, which could be attributed to the decomposition of CDs, copolymers and the remained oxygen-containing groups. And the second from 420 to 700 °C is attributed to pyrolysis of the carbon skeleton of graphene sheets.[20] According to the final weight loss of CD-G (45%) and copolymer (97%), it can be calculated that the weigh percentage of AZO-(PDMA-*b*-PNIPAM) block copolymer in HGIC is as high as 66%.

Raman spectroscopy is employed to investigate the structural changes that occur in graphene modification. In general, the D-band is assigned to the $sp^3$ carbons ($\sim$1344 $cm^{-1}$) in graphene sheets, and G-band corresponds to $sp^2$ carbon stretching modes in carbonaceous material.[21] The Raman spectra of GO, CD-G, and HGIC are shown in Figure S5, Supporting Information. Two prominent peaks are observed around 1344 and 1600 $cm^{-1}$, assigned to the D band and G band, respectively. The G-band of CD-G and HGIC occur at 1597 $cm^{-1}$, which downshifts 3 $cm^{-1}$ compared to that of GO and becomes close to the value of graphite. This is caused by the thermal reduction of GO during the amine-epoxide ring-opening reaction, similar to that reported in literature.[22]

In order to investigate the CD modification and polymer functionalization of graphene in detail, XPS is employed. Figure 2a provides the survey spectra of GO, CD-G, and HGIC from 0 to 800 eV. Notable peaks are observed at binding energy of 285 and 533 eV, corresponding to C 1s and O 1s, respectively,[23] while slight reflections at 169 and 400 eV are assigned to S 2p and N 1s, respectively. Besides, based on the number ratio of N to C atoms of GO, it is calculated that there is one $\beta$-CD per 67 carbon atoms of GO, i.e. 1.66 $nm^2$ occupied by one CD (Table S1, calculation details in Supporting Information). Considering the relatively large diameter of CDs (ca. 1 nm), the density of CDs on graphene sheets is sufficiently high. Moreover, XPS survey of HGIC shows significant amount of N 1s comparing to that of CD-G, which is originated from AZO-(PDMA-*b*-PNIPAM) block copolymers, verifying the success of noncovalent polymer functionalization of graphene sheets by inclusion complexation.

Figure 2b shows O 1s XPS spectra of GO, CD-G, and HGIC. The O 1s spectrum of GO appears at 532.8 eV, assigned to the

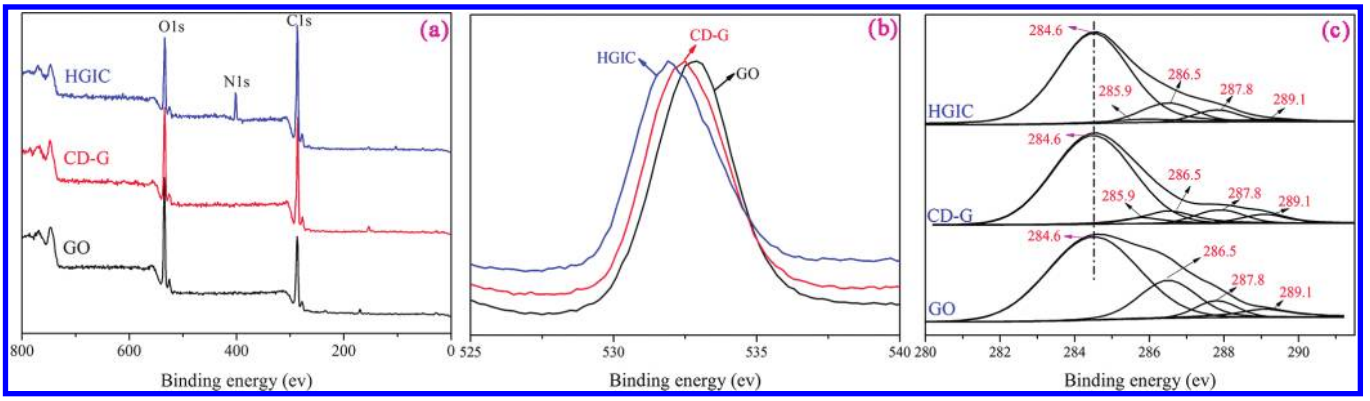


**Figure 2.** XPS (a) survey spectra and (b) O 1s and (c) C 1s spectra of GO, CD-G, and HGIC.

forms of C−O−C and C═O. After reaction with EDA-CD, the O 1s spectrum of CD-G shifts to 532.3 eV, in the form of C−OH, C−O−C, and C═O from CD and the remained oxygen in graphene. Comparing to CD-G, the O 1s spectrum of HGIC further shifts to 531.7 eV, because of the large amount of C═O in AZO-(PDMA-*b*-PNIPAM) block copolymers.

C 1s XPS spectra of the samples obtained in high resolution are presented in Figure 2c. Briefly, the spectrum of GO clearly indicates a considerable degree of oxidation with four components that correspond to carbon atoms: the nonoxygenated ring C (284.6 eV), in the form of C−O (286.5 eV), C═O (287.8 eV), and O−C═O (289.1 eV).[24,25] After reaction with EDA-CD, C 1s XPS spectrum of the CD-G exhibits similar oxygen functionalities, including the remaining oxygen-containing groups of the graphene sheets and the oxygen-containing groups of CDs. However, it shows a significant intensity decrease of the peak at 286.5 eV, that of the epoxy/ether group, which proves that most of the epoxy functional groups on GO are successfully removed. Meanwhile, an increase of the proportion of the nonoxygenated ring C is observed. This result confirms the recovery of the $sp^2$ planar structure in CD-G, comparing to GO.

AFM images of the exfoliated GO, CD-G, and HGIC on freshly cleaved mica surfaces, obtained by drop-casting, are shown in Figure 3 and S6 (Supporting Information). In order to observe the exact distance between the layers, aqueous dispersions of the samples at rather low concentration (0.01 mg/mL) were employed. In this work, all of the observed sheets showed irregular shapes with sizes ranging from 0.1 to 1 $\mu$m. The cross-sectional analyses of the height profiles showed that the thickness of the CD-G sheets were about 1.6 nm (Figure 3b and S6-(Supporting Information)), larger than that of its precursor, the well exfoliated GO sheets, which were around 1 nm (Figure 3a). This thickness increase of CD-G could be attributed to the CD layer attached onto the graphene surface from both sides. Besides, CD-G gave clearer and smooth surface compared to GO, indicating the successful restore of $sp^2$ carbons by chemical procedures as well as homogeneous coverage of CD molecules on the surface. Furthermore, the typical thickness of single-layered HGIC, which contained noncovalent modification of AZO-(PDMA-*b*-PNIPAM) block copolymers, increased to ca. 2.2 nm with a rather flat surface profile (Figure 3c) at room temperature, which indicated that the copolymer chains are uniformly grafted on the graphene surfaces. It is worth to mention that, cross-sectional measurements for height (Figure S6 (Supporting Information)) have been done triply with reproducible results for CD-G and HGIC, due to the extra thin and flat property of the graphene sheets. It is well-known that the thermo sensitive polymer, PNIPAM becomes hydrophobic and begins to aggregate when the temperature is above its LCST (lower critical solution temperature). As shown in Figure 3d, the thickness of HGIC obtained at 40 °C, above LCST, was dramatically increased, from 2.2 nm to a wide range, approximately from 4 to 11 nm. This increase of thickness could be attributed to, the aggregation of the single layer of graphene sheets to multiple layers, as well as the micelle-like structure formation of the neighboring copolymer chains above LCST. In short, the effect of polymer aggregation on graphene surface is obvious.

TEM is not only useful to assess the dispersion state of graphene sheets, but also to present a comparison of the morphologies of GO, CD-G, and HGIC. As shown in TEM image, GO sheets are very thin and have wrinkles and folded regions, indicating the random overlay of the individual sheets (Figure 4a). After reaction with EDA-CD, CD-G becomes more transparent and has much smaller contrast than that of GO. This further supports the recovered $sp^2$ planar surface of graphene. Steric hindrance between adjacent CDs might also contribute to this flattened surface, since the CD density is rather high (Figure 4b). Furthermore, in the TEM image of HGIC at room temperature (Figure 4c), no obvious black points on the surface of CD-G are observed, which indicates that the AZO-(PDMA-*b*-PNIPAM) block copolymer chains are well distributed on graphene sheets with uniform brushing density. This is consistent with the results from AFM. As observed from Figure 4d, above LCST, PNIPAM blocks of the copolymers begin to aggregate, resulting in uneven surface characters.

**Formation of HGIC Hydrogels and Their Rheology Properties.** HGIC was prepared through noncovalent interactions between graphene sheets as 2D backbone and AZO-(PDMA-*b*-PNIPAM) block copolymers as brushes attached to the basal planes with the PNIPAM block as the outer layer. It is well-known that when the temperature increases to the LCST of PNIPAM, it switches from a hydrophilic, coil state to a hydrophobic, collapsed state.[26] In our previous study,[11] the HIC structure, which had the nanoparticles as the core and the same block copolymers as the shell, was proved to form hydrogels upon heating due to the formation of the domains of collapsed PNIPAM chains. The gelation process was pretty slow and often took tens of minutes above the LCST. And the gelation temperature was higher than the LCST, typically around 40 °C.[11a] As expected, HGIC also formed hydrogels at elevated temperature as desired. However, with the same copolymer as that used in HIC, HGIC did show much faster sol−gel transition, typically

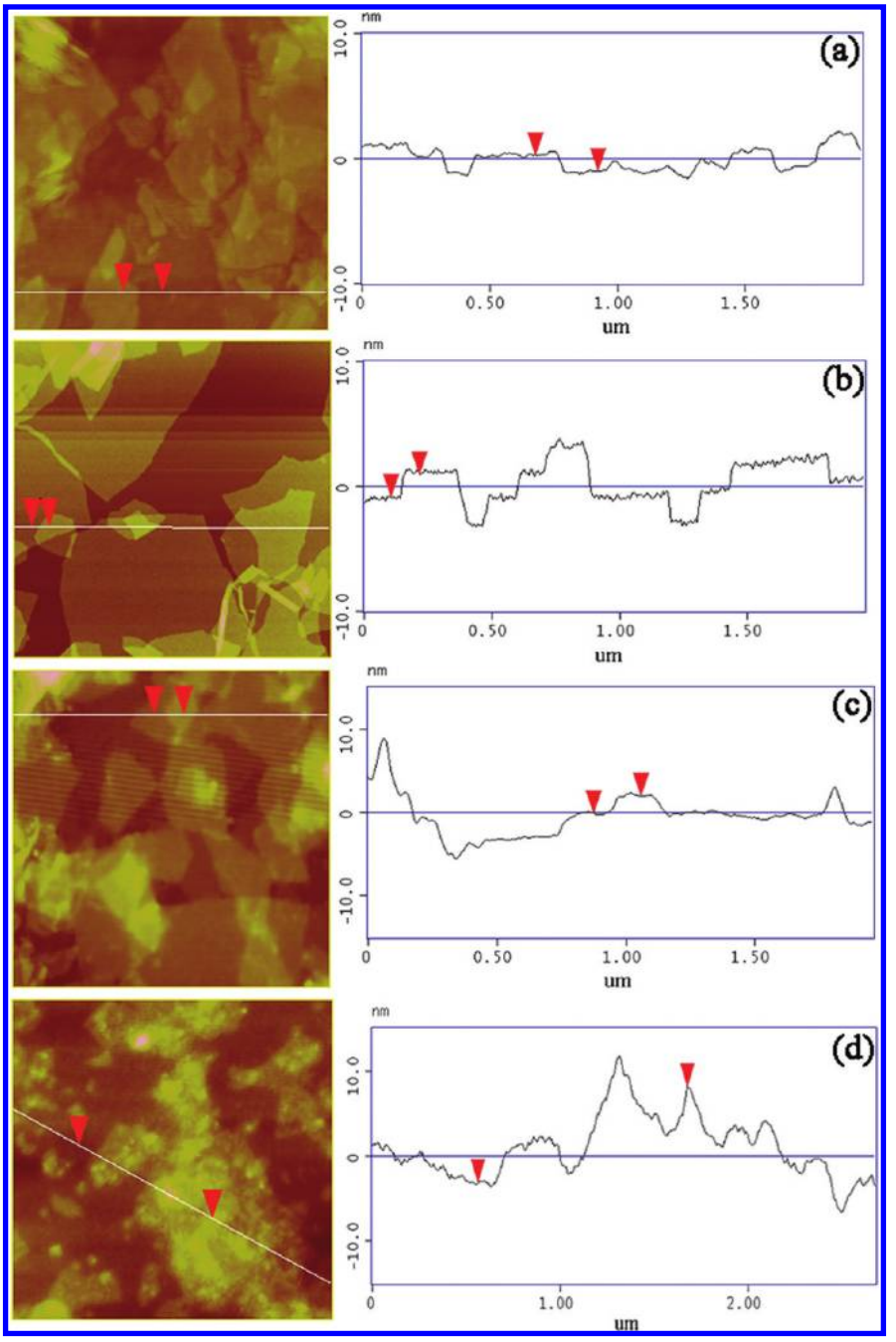


**Figure 3.** AFM images and height profiles of (a) GO, (b) CD-G, and HGIC (c) at room temperature and (d) at 40 °C above the LCST.

about 1−2 min only around the LCST. And the HGIC was able to form hydrogels at temperatures even lower the LCST (typical LCST result of the block copolymer in Figure S7). This inspired us to try to explore this difference in detail. In this part, seven AZO-(PDMA-*b*-PNIPAM) block copolymers with different DPs have been used (Table 2). The copolymers are labeled and arranged according to the DP (degree of polymerization) ratio of PDMA to PNIPAM ($R_m$), due to the reasons discussed below. The block copolymers cover a large range of $R_m$, i.e., from **P1** to **P7**, $R_m$ increases from 0.55 to 4.59.

The formation of hydrogels was monitored by dynamic rheological measurement. We now discuss the result of **HGIC-3** as an example first. The oscillatory temperature sweep profiles of the aqueous solution of copolymer **P3** (10 wt %, weight percentage, the same below) and **HGIC-3** (10 wt % and 15 wt %) are shown in Figure 5. It is well-known that the polymer solution exhibits linear viscous response ($G'' > G'$) and polymeric gel shows dominantly elastic response ($G' > G''$). The temperature at which $G'$ (elastic modulus) curve intersects that of $G''$ (viscous modulus) indicates the sol−gel transition. As a control, $G'$ and $G''$ of **P3** solution were very low and varied little with temperature, and $G''$ was always higher than $G'$ over the temperature range. This indicated that **P3** (10 wt %) was always at sol state and never turned to gel upon heating. $G'$ and $G''$ of **HGIC-3** at concentrations of 10 wt % and 15 wt % exhibited viscous properties below 28 °C. When the temperature was close to

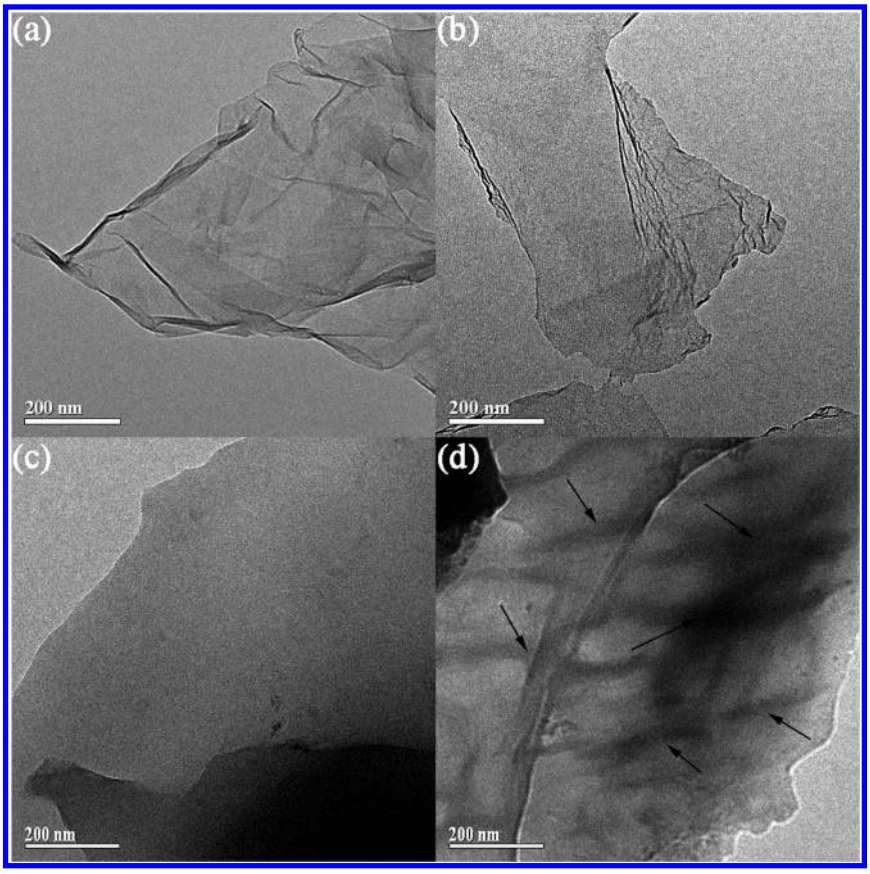


**Figure 4.** TEM images of (a) GO, (b) CD-G, (c) HGIC at room temperature and (d) above LCST. Aggregated copolymers on graphene surface are shown by arrows.

**Table 2. DP of AZO-(PDMA$_m$-*b*-PNIPAM$_n$) Block Copolymers, PNIPAM Content $R_m$ (DP$_m$:DP$_n$), the Gelation Temperature ($T_{gel}$), and the Temperature of the Onset of Viscosity Increase ($T_\eta$) of Their Corresponding HGIC (Concentration 10 wt %)**

| copolymers[a] | HGIC | DP$_m$[b] | DP$_n$[b] | DP$_m$ + DP$_n$[b] | $R_m$ | $T_{gel}$[c] | $T_\eta$[d] |
|---|---|---|---|---|---|---|---|
| **P1** | **HGIC-1** | 122 | 223 | 345 | 0.55 | 29.8 | 29.3 |
| **P2** | **HGIC-2** | 191 | 267 | 458 | 0.72 | 30.6 | 30.4 |
| **P3** | **HGIC-3** | 104 | 138 | 242 | 0.75 | 31.4 | 32.0 |
| **P4** | **HGIC-4** | 109 | 89 | 198 | 1.22 | 34.4 | 34.4 |
| **P5** | **HGIC-5** | 230 | 133 | 363 | 1.73 | - | 36.1[e] |
| **P6** | **HGIC-6** | 219 | 84 | 303 | 2.61 | - | 39.9[e] |
| **P7** | **HGIC-7** | 418 | 91 | 509 | 4.59 | - | - |

[a] Experimental detail and characterization of **P3** and **P7** are in Supporting Information, those of the other copolymers were in ref 11a. [b] Experimental DP. [c] Temperature at which $G' = G''$. [d] Temperature to which turning point of viscosity curve corresponds. [e] Gel did not form.

the LCST of PNIPAM, a sharp increase of $G'$ and $G''$ was observed, which was associated with the gelation process. Both $G'$ and $G''$ increased by three or 4 orders of magnitude and then leveled off within 5 °C. Besides, the increase rate of $G'$ was much higher since the elastic properties started to dominate. The temperature at which $G'$ became equal to $G''$ was noted as gelation temperature $T_{gel}$. As shown in Figure 5a, $T_{gel}$ of **HGIC-3** was 31.4 and 29.8 °C at the concentration of 10 wt % and 15 wt %, respectively. When temperature reached $T_{gel}$, **HGIC-3** turned into gel state, due to the formation of the cross-linked network caused by the aggregation of PNIPAM. It was noted that both $T_{gel}$ values were lower than the LCST of PNIPAM.

Meanwhile, viscosity of **P3** and **HGIC-3** measured in the same dynamic rheology test is shown in Figure 5b. The viscosity of **P3** (10 wt %) varied little with increasing temperature from 25 to 40 °C. The viscosity of HGIC solution was also low and varied little with temperature at the beginning. When the temperature was increased further, an abrupt viscosity enhancement occurred. So in each of the viscosity-temperature curve, there is a clear turning point, which is noted as $T_\eta$. For the cases of concentrations of 10% and 15%, the respective $T_\eta$ were 32.0 and 28.6 °C, very close to the corresponding $T_{gel}$ values.

Figure 6 presents the dynamic rheological behavior of the **HGIC-N** ($N$ = 1, 2, 4, 5) solutions listed in Table 2 as a function of temperature at the same concentration of 10 wt %. Generally, the solutions showed similar behavior as that of **HGIC-3** in Figure 5. $G'$ and $G''$ of **HGIC-1** gel were almost 4 orders of magnitude higher than that of the corresponding solution. It was very encouraging to observe this huge enhancement of the modulus of HGIC obtained with the aid of noncovalent modification to graphene, which demonstrated the high gelation efficiency of our HGIC suprastructure. More interestingly, the gelation temperature $T_{gel}$ of the series of HGIC increased regularly from 30 to 37 °C from **HGIC-1** to **HGIC-5**, i.e. in parallel with the increase of the ratio $R_m$ of the copolymers.

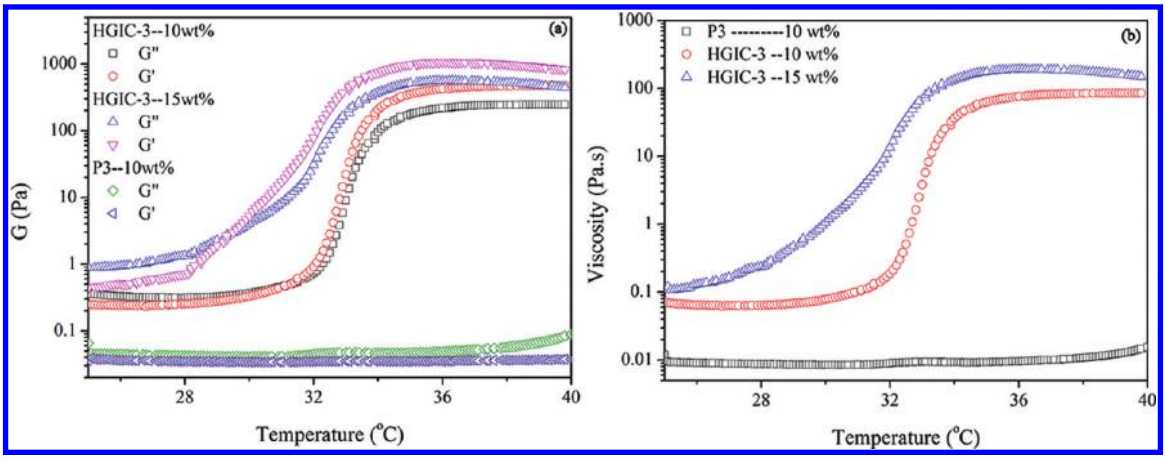


**Figure 5.** Dynamic rheology measurement of $G'$, $G''$ (a) and viscosity (b) of **P3** (10 wt %) and **HGIC-3** (10 wt % and 15 wt %) in aqueous solution as a function of temperature (constant shear frequency: 1 Hz).

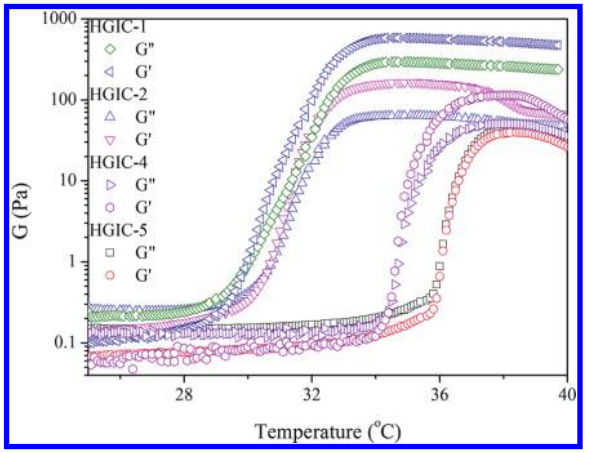


**Figure 6.** $G'$ and $G''$ moduli of **HGIC-N** ($N$ = 1, 2, 4, 5, concentration 10 wt %) as a function of temperature (constant shear frequency: 1 Hz).

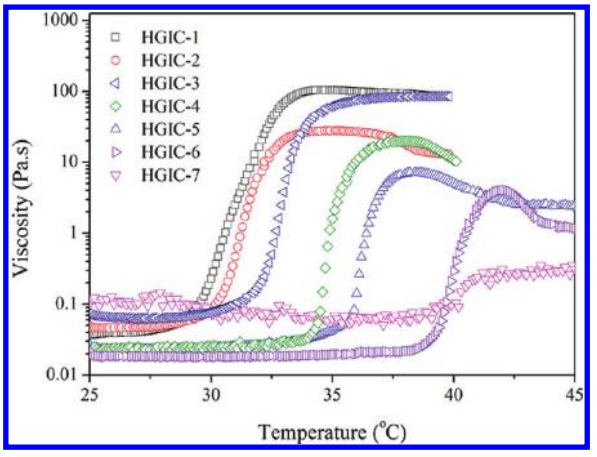


**Figure 7.** Viscosity variations of **HGIC-N** ($N$ = 1−7) in aqueous solution as a function of temperature (constant shear frequency: 1 Hz).

Figure 7 presents the viscosity−temperature curves for all the solutions of **HGIC-N** ($N$ = 1−7). Except **HGIC-7**, which has the least content of PNIPAM, all of them show similar viscosity variation with temperature exhibiting clear turning points $T_\eta$ in the viscosity-temperature curves. And $T_\eta$ for each of the HGIC solutions is very close to the corresponding $T_{gel}$ (Table 2). Although the viscosity increase of **HGIC-5** and **HGIC-6** with temperature is obvious, the obtained viscous solutions at the end of the experiment cannot be called "hydrogel" since the absolute value of the viscosity is rather low and their $T_{gel}$ are not observed. For the hybrid complexes made of other copolymers, i.e. from **HGIC-1** to **HGIC-4**, not only an abrupt viscosity increase is observed, but also hydrogel formation can be proved by tube-reverse test at elevated temperature.

The most remarkable result obtained from the rheology measurements of the series of HGIC solutions is that both $T_{gel}$ and $T_\eta$ indicative of the gel formation, vary with the block copolymer structure following the ratio $R_m$, i.e., the larger the ratio, which means the relatively smaller content of PNIPAM block, the harder the gelation formation. And other parameters of the copolymer, such as the total length of the copolymer and the polymerization degree of PNIPAM block do not show such clear and monotonic correlation with the gelation formation. This unique character of gelation is possibly associated with the peculiar structure of graphene, which is very different from the other inorganic constituents used in hybrid hydrogels.[11] As just fully characterized, the HGIC has a smooth block copolymer layer on the graphene surface. The size of the ultrathin and flexible graphene sheet is around 0.1−1 $\mu$m, which holds numerous block copolymer chains ($M_w$ = 20K−50K) with a high density, i.e., one chain for every 1.6 nm$^2$ of surface area (Supporting Information). When temperature is increased to close the LCST, PNIPAM blocks become hydrophobic and collapse. Once the hydrophobic PNIPAM blocks from copolymer chains attaching to different sheets aggregate together forming common domains (Figure 8), the adjacent graphene sheets would be connected and then lead to network formation. In other words, the interchain collapse of PNIPAM initiates the graphene sheets connection to form hydrogel network. Considering the large size of the graphene sheets, which makes the sheets rather closer to each other than that between the nanoparticles in our previous HIC systems,[11] and the rather high density of the copolymers on the graphene surface, the intergraphene connection is much easier to initiate. That is why the gelation of HGIC could be realized faster and at lower temperature than that of HIC. In this procedure, the key factor is still the temperature-induced chain collapse of PNIPAM blocks. Obviously, the longer the ever-hydrophilic

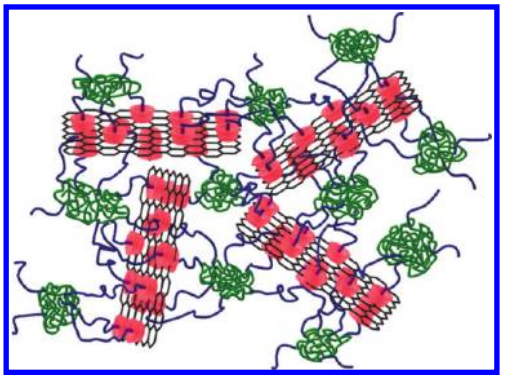

**Figure 8.** Possible hydrogel structure made of HGIC.

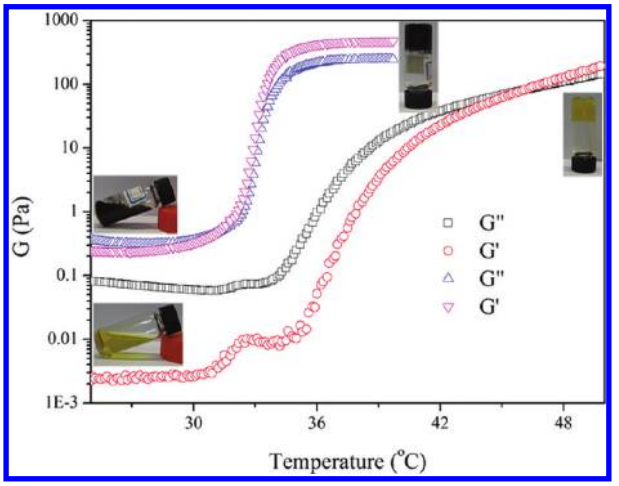


**Figure 9.** Variation of $G'$ and $G''$ of the **HGIC-3** and HIC[11a] at a constant shear frequency of 1 Hz prepared by CD@CdS at the (solid content, 10 wt %; temperature increase rate, 1 °C/min).

PDMA block and the shorter the temperature-sensitive PNIPAM blocks, the harder the sol−gel transition, i.e., the higher gelation temperature is needed. The dependence of gelation temperature on the ratio $R_m$ reflects that the aggregation ability of the PNIPAM block in the space between adjacent graphene sheets determines the gelation behavior. The difference in gelation behavior between HIC and HGIC can be clearly seen in Figure 9. $T_{gel}$ of **HGIC-3** is around 31.4 °C, much lower than that of the HIC (~46 °C) when the same temperature increase rate, the same block copolymer ($R_m$) at the same concentration was used. This significant decrease of $T_{gel}$ of HGIC indicates the unprecedented advantage of graphene sheets to construct 3D network structure of hydrogel than the inorganic nanoparticles. In addition, HGIC also preserves the sol−gel thermo reversibility and responses to supramolecular competition, which is not the key point of this paper (results in Figure S8 and S9, Supporting Information).

## CONCLUSION

In this paper, we demonstrated the noncovalent modification of block copolymers of AZO-PDMA-*b*-PNIPAM to graphene surface by inclusion complexation leading to hybrid graphene inclusion complex (HGIC). This new suprastructure forms hydrogel on heating. This stimuli responsive hydrogel with inherent biocompatibility of carbon materials may have many important potential applications in the fields of biotechnology, such as drug delivery and tissue scaffolds. Rheology studies reveal that gelation temperature of HGIC ($T_{gel}$) increases with the ratio of degree of polymerization of PDMA block to PNIPAM block, $R_m$, in the polymers. On the basis of these results, a new possible mechanism of sol−gel transition of HGIC has been proposed. The interchain collapse of PNIPAM on heating initiates and mediates the intergraphene connection. This mechanism may cause much interest and attracts more attention on various graphene-based polymeric composites, which are currently undergoing in our laboratory.

## EXPERIMENTAL SECTION

**Materials.** Graphite powders (99 wt %, 320 mesh) were supplied by Shanghai Yi Fan graphite CO LTD, which was characterized by elemental analysis before use. Graphite oxide was prepared according to the literature report[27] and purified by dialysis for 1 week to remove any impurities. *N*-Isopropylacrylamide (NIPAM, recrystallized three times from benzene/hexane (65:35 v/v) prior to use) and *N*,*N*-dimethylacrylamide (DMA, distilled under reduced pressure before polymerization) were purchased from Tokyo Kasei Kagyo Co. 4-Phenylazophenol (97%) was purchased from Alfa Aesar. $\beta$-cyclodextrin ($\beta$-CD, CP, recrystallized twice from deionized water) and azodiisobutyronitrile (AIBN, CP, recrystallized from ethanol before use) were supplied by Sinopharm Chemical Reagent Co. Other reagents were of analytical grade and used as received. All aqueous solutions were prepared by deionized water.

**Measurement and Characterization.** $^1$H NMR spectra were recorded with a JEOL ECA-400 spectrometer. Samples were prepared in $CDCl_3$-*d*. Gel permeation chromatography (GPC) analysis was carried out with a Waters Breeze 1525 GPC analysis system with two PL mix-D columns, using DMF with 0.5 M LiBr as eluents at the flow rate of 1 mL/min at 80 °C. PEO calibration kit (purchased from TOSOH) was used as the calibration standard. UV−vis spectra were recorded in a conventional quartz cell (light path 10 mm) on a Perkin-Elmer Lambda 35 spectrophotometer. AFM images of the samples deposited from a dilute aqueous dispersion (~0.01 mg/mL) onto a freshly cleaved mica surface were taken in tapping mode with a VEECO Dimensions 3100 instrument and a nanoscope IV controller. TEM pictures were taken by JEM 2011 transmission electron microscope from JEOL operating at 200 kV. UV−vis spectra were recorded in a conventional quartz cell (light path 10 mm) on UV-2550 Spectrophotometer from Shimadzu, Japan. TGA measurements were carried out on a Perkin-Elmer Pyris-1 series thermal analysis system under a flowing nitrogen gas at a scan rate of 20 °C $min^{-1}$ from 100 to 700 °C. All the samples were heated to 100 °C for a while to ensure that all the residual water was removed during test period. Raman measurements were carried out on LabRam-1B microscope Raman spectrum instrument (Dilor, France). The source exciting laser wavelength is 632.8 nm and the power is 3 mW. The instrument employed for XPS studies was a Perkin-Elmer PHI 5000C ESCA system with Al K$\alpha$ radiation operated at 250 W. The shift of the binding energy due to relative surface charging was corrected using the C 1s level at 284.6 eV as an internal standard. The rheological behavior of the samples was measured by Bohlin GeminiHRnano (Malvern, U.K.), fitted with a parallel plate (diameter 40 mm) and circulating environmental system for temperature control. The gap distance between the two parallel plates was fixed at 0.2 mm. The gel formation process was investigated by increasing temperature at a rate of 1 °C/min. Dynamic rheology measurements were performed by oscillatory temperature sweeps (stress-controlled) at an oscillation frequency of 1 Hz and the deformation of 0.1. The $G'$, $G''$, and viscosity variation data were collected in the same dynamic rheology experiment with the same temperature increase rate.

**Synthesis of β-CD Functionalized Graphene Nanosheets.** Ethylenediamino-β-cyclodextrin (EDA-CD) was prepared following the reported procedure.[28] β-CD functionalized graphene (CD-G) was synthesized by an epoxide ring-opening reaction between GO and EDA-CD. Typically, 150 mg of GO was loaded in a 500 mL round-bottom flask, and 300 mL deionized water was then added. After stirring and ultrasonication for more than 2 h, 200 mg of KOH and 1 g of EDA-CD were added to the solution. The mixture was stirred for 10 min at room temperature to ensure complete dissolution. Then it was transferred to an 80 °C oil bath and stirred for 24 h. After the reaction, a homogeneous black solution was obtained. There was almost no precipitation after centrifugation at 12000*g* for 30 min. The solution was concentrated under a reduced pressure. The residue was transferred to a dialysis bag (molecular weight cut off: $1.4 \times 10^4$). Purification of CD-G was carried out in a basic aqueous solution (pH = 12) for 3 d. The final solution containing CD-G inside the dialysis bag was neutralized by dialysis with neutral water for 5 d. The remaining black solid was centrifuged and dried under vacuum.

**Preparation of Hybrid Graphene Inclusion Complex and Formation of Responsive Hydrogel.** A predetermined amount of CD-G was dispersed in water (pH 8−9). Then the corresponding amount of AZO-(PDMA-*b*-PNIPAM) was added, where the molar ratio of β-CD in CD-G and AZO in AZO-(PDMA-*b*-PNIPAM) was 1:1. The obtained solution was stirred for more than 24 h to ensure sufficient interactions between β-CD and AZO. The hybrid graphene inclusion complex was obtained through centrifugation and washed with water. It was then dried *in vacuo* for further characterization.

To prepare the responsive hydrogel, the above HGIC solution at higher concentration (10 wt % or 15 wt %) was heated close to the LCST of PNIPAM block of AZO-(PDMA-*b*-PNIPAM) block copolymers for a couple of minutes to form hydrogel. The apparent formation of the hydrogel was examined by a tube inversion method.

## ■ ASSOCIATED CONTENT

**Supporting Information.** Figures S1−S11, showing the synthetic route, GPC traces, $^1$H NMR spectra, TGA results, Raman spectra, AFM images and height profiles, a typical LCST profile, and variation of elastic and viscous moduli, Table S1, giving atomic concentrations of graphitic derivatives, and a discussion of the calculation of the degree of functionalization of graphene sheet. This material is available free of charge via the Internet at http://pubs.acs.org.

## ■ AUTHOR INFORMATION

**Corresponding Author**

*E-mail: (M.J.) mjiang@fudan.edu.cn; (G.C.) guosong@fudan.edu.cn.

## ■ ACKNOWLEDGMENT

National Natural Science Foundation China (No. 20834004 and 20904005) and Ministry of Science and Technology of China (2009CB930402 and 2011CB932503) are acknowledged for financial support.

## ■ REFERENCES

(1) (a) Haraguchi, K. *Polym. J.* **2011**, *43*, 223–241. (b) Wang, C.; Flynn, N. T.; Langer, R. *Adv. Mater.* **2004**, *16*, 1074–1079. (c) Sui, K.; Gao, S.; Wu, W.; Xia, Y. *J. Polym. Sci., Part A., Polym. Chem.* **2010**, *48*, 3145–3151. (d) Shi, M. K.; Spinks, G. M.; Shin, S. R.; Kim, S. I.; Kim, S. J. *Adv. Mater.* **2009**, *21*, 1712–1715.

(2) Guo, M.; Jiang, M.; Pispas, S.; Yu, W.; Zhou, C. *Macromolecules* **2008**, *41*, 9744–9749.

(3) (a) Germ, A. K.; Novoselov, K. S. *Nat. Mater.* **2007**, *6*, 183–191. (b) Allen, M. J.; Tung, V. C.; Kaner, R. B. *Chem. Rev.* **2010**, *110*, 132–145.

(4) (a) Bai, H.; Li, C.; Wang, X.; Shi, G. *Chem. Commun.* **2010**, *46*, 2376–2378. (b) Xu, Y.; Sheng, K.; Li, C.; Shi, G. *ACS Nano* **2010**, *7*, 4324–4330. (c) Sheng, K.; Xu, Y.; Li, C.; Shi, G. *New. Carbon. Mater.* **2011**, *26*, 9–15. (d) Xu, Y.; Wu, Q.; Sun, Y.; Bai, H.; Shi, G. *ACS Nano* **2010**, *4*, 7358–7362. (e) Lo, C. W.; Zhu, D.; Jiang, H. *Soft Matter* **2011**, *7*, 5604–5609. (f) Huang, C.; Bai, H.; Li, C.; Shi, G. *Chem. Commun.* **2011**, *47*, 4962–4964. (g) Sun, S.; Wu, P. *J. Mater. Chem.* **2011**, *21*, 4095–4097.

(5) Alzari, V.; Nuvoli, D.; Scognamillo, S.; Piccinini, M.; Gioffredi, E.; Malucelli, G.; Marceddu, S.; Sechi, M.; Sanna, V.; Mariani, A. *J. Mater. Chem.* **2011**, *21*, 8727–8733.

(6) Zu, S.; Han, B. *J. Phys. Chem. C* **2009**, *113*, 13651–13657.

(7) (a) Potts, J. R.; Dreyer, D. R.; Bielawski, C. W.; Ruoff, R. S. *Polymer* **2011**, *52*, 5–25. (b) Kim, H.; Abdala, A. A.; Macosko, C. W. *Macromolecules* **2010**, *43*, 6515–6530.

(8) Dreyer, D. R.; Park, S.; Bielawski, C. W.; Ruoff, R. S. *Chem. Soc. Rev.* **2010**, *39*, 228–240.

(9) (a) Compton, O. C.; Nguyen., S. T. *Small* **2010**, *6*, 711–723. (b) Dreyer, D. R.; Bielawski, C. W. *Chem. Sci.* **2011**, *2*, 1233–1240. (c) Dreyer, D. R.; Ruoff, R. S.; Bielawski, C. W. *Angew. Chem., Int. Ed.* **2010**, *49*, 9336–9344.

(10) (a) Wang, D.; Ye, G.; Wang, X.; Wang, X. *Adv. Mater.* **2011**, *23*, 1122–1125. (b) Fang, M.; Wang, K.; Lu, H.; Yang, Y.; Nutt, S. *J. Mater. Sci.* **2009**, *19*, 7098–7105. (c) Lee, S. H.; Dreyer, D. R.; An, J.; Velamakanni, A.; Piner, R. D.; Park, S.; Zhu, Y.; Kim, S. O.; Bielawski, C. W.; Ruoff, R. S. *Macromol. Rapid Commun.* **2010**, *31*, 281–288. (d) Huang, Y. J.; Qin, Y. W.; Zhou, Y.; Niu, H.; Yu, Z. Z.; Dong, J. Y. *Chem. Mater.* **2010**, *22*, 4096–4102. (e) Deng, Y.; Li, Y.; Lang, M.; Huang, X. *J. Polym. Sci., Part A: Polym. Chem.* **2011**, *49*, 1582–1590. (f) Pan, Y.; Bao, H.; Sahoo, N. G.; Wu, T.; Li, L. *Adv. Funct. Mater.* **2011**, *21*, 2754–2763.

(11) (a) Liu, J.; Chen, G.; Guo, M.; Jiang, M. *Macromolecules* **2010**, *43*, 8086–8093. (b) Du, P.; Liu, J.; Chen, G.; Jiang, M. *Langmuir* **2011**, *27*, 9602–9608.

(12) Chen, G.; Jiang, M. *Chem. Soc. Rev.* **2011**, *40*, 2254–2266.

(13) Hummers, W. S.; Offeman, R. E. *J. Am. Chem. Soc.* **1958**, *80*, 1339–13340.

(14) Guo, Y.; Guo, S.; Ren, J.; Zhai, Y.; Dong, S.; Wang, E. *ACS Nano* **2010**, *4*, 4001–4010.

(15) (a) Yang, H.; Li, F.; Shan, C.; Han, D.; Zhang, Q.; Niu, L.; Ivaska, A. *J. Mater. Chem.* **2009**, *19*, 4632–4638. (b) Yang, H.; Shan, C.; Li, F.; Han, D.; Zhang, Q.; Niu, L. *Chem. Commun.* **2009**, 3880–3882.

(16) Yoshida, N.; Seiyama, A.; Fujimoto, M. *J. Phys. Chem.* **1990**, *94*, 4254–4259.

(17) Zhu, Y.; Higginbotham, A. L.; Tour, J. M. *Chem. Mater.* **2009**, *21*, 5284–5291.

(18) Kumar, G. S.; Neckers, D. C. *Chem. Rev.* **1989**, *89*, 1915–1925.

(19) Stankovich, S.; Dikin, D. A.; Piner, R. D.; Kohlhaas, K. A.; Kleinhammes, A.; Jia, Y.; Wu, Y.; Nguyen, S. T.; Ruoff, R. S. *Carbon* **2007**, *45*, 1558–1565.

(20) He, H.; Gao, C. *Chem. Mater.* **2010**, *22*, 5054–5064.

(21) Ferrari, A. C.; Meyer, J. C.; Scardaci, V.; Casiraghi, C.; Lazzeri, M.; Mauri, F.; Piscanec, S.; Jiang, D.; Novosclow, K. S.; Roth, S.; Geim, A. K. *Phys. Rev. Lett.* **2006**, *97*, 187401(1)–187401(5).

(22) Kudin, K. N.; Ozbas, B.; Schniepp, H. C.; Prud'homme, R. K.; Aksay, I. A.; Car, R. *Nano Lett.* **2008**, *8*, 36–41.

(23) Bekyarova, E.; Itkis, M. E.; Ramesh, P.; Berger, C.; Sprinkle, M.; de Heer, W. A.; Haddon, R. C. *J. Am. Chem. Soc.* **2009**, *131*, 1336–1337.

(24) Zhou, X.; Zhang, J.; Wu, H.; Yang, H.; Zhang, J.; Guo, S. *J. Phys. Chem. C.* **2011**, *115*, 11957–11961.

(25) Iwase, A.; Ng, Y. H.; Ishiguro, Y.; Kudo, A.; Amal, R. *J. Am. Chem. Soc.* **2011**, *133*, 11054–11057.

(26) Heskinsa, M.; Guillet, J. E. *J. Macromol. Sci., Pure Appl. Chem.* **1968**, *2*, 1441–1445.
(27) (a) Kovtyukhova, N. I.; Ollivier, P. J.; Martin, B. R.; Mallouk, T. E.; Chizhik, S. A.; Buzaneva, E. V.; Gorchinskiy, A. D. *Chem. Mater.* **1999**, *11*, 771–778. (b) Bai, H.; Xu, Y.; Zhao, L.; Li, C.; Shi, G. *Chem. Commun.* **2009**, *7*, 1667–1669.
(28) Ohashi, H.; Hiraoka, Y.; Yamaguchi, T. *Macromolecules* **2006**, *39*, 2614–2620.